Beam Physics Note
TRI-BN-22-10
April 13, 2022

Report on TRIUMF e-LINAC ELBT:ACCT Current Monitoring System

H. W. Koay

TRIUMF

Abstract: This work reports the procedure to practically implement ACCT along the ELBT beamline.

1 Objectives

Due to the limitations (as listed below) of the capacitive RF shield in monitoring the beam current effectively , this report aims to summarize the procedures to calibrate and analyze the output of an AC Current Transformer (ACCT) current monitoring system at the ELBT beamline. In future, this ACCT shall be used to replace the RF shield for online current monitoring.

Current Limitations:

- The current implementation required that the gun RF properties are locked when the EOECM is engaged, preventing us form implementing a feed-back mechanism on the gun RF forward power.
- The setup of the RF shield calibration is tedious and time-consuming.
- The beam energy has to be manually input by operators.

Advantages of ACCT

- Can measure a broad frequency range (from a few Hz up to a few MHz)
- output current is sufficient for direct computation (No need an amplifier)
- High accuracy (up to 0.1%)
- Independent of longitudinal beam structure (bounded by the frequency range)
- Repeated calibration before use is not required once the initial calibration is done (Easy implementation)

2 Procedures and Methods

1. Connect the ACCT output to a digital oscilloscope. In this work, Rohde&Schwarz RTB2004 (IP address : 142.90.103.232) is used.

2. Change the manipulating variables and collect data output from the oscilloscope.

   Manipulating variables: Pulse length (Duty factor), Beam frequency

   Responding variables: Output waveform, voltage, pulse width

3. Calibrate the output by connecting an AC current source (Agilent 33250A) to the calibration winding (CAL winding at 50 Ω). The input current is then determined from the input voltage $I = \frac{V}{R}$.

4. Analyze the data offline using GNU Octave.

3 Results and Discussions

A sample output of from ACCT is shown in Fig. 1.

Figure 1: Sample output from ACCT. It corresponds to a single pulse beam at *(left)* 10 Hz, duty factor (DF) = 5%, *(right)* 1 Hz, DF = 20%.

The output shows a significant distortion of waveform when the pulse width is longer than ∼ms. According to the manual, the drooping percentage is about 2%. When the taken data for long pulses is fitted with a function

$$V(x) = -V_o \cdot B^x$$

for $x = 100$ ms, the decay constant is about 1.5 %, which is close to the data provided by the company.

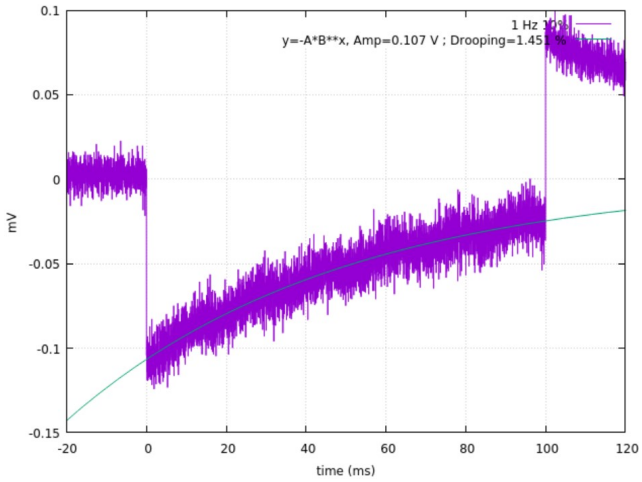

Figure 2: Fitting a drooping output from ACCT for pulse width of 100 ms. The fitted function shows a drop of about 1.5% per ms, which agrees with the nominal value of 2% provided by the manufacturer.

3.1 Signal transformation of ACCT

The distorted drooping wave structure is a result of the coil inductance. Given the y_{in} is the input signal from the beam, whil y_{out} is the output signal from the ACCT, and H is the transfer function of the system, the signal transformation can be simplified as

$$\begin{aligned}
\mathcal{L}(y_{out}) &= \mathcal{L}(y_{in}) \cdot H \\
H_{high} &= \frac{j\omega/\omega_C}{1 + j\omega/\omega_C} \\
H_{low} &= \frac{1}{1 + j\omega/\omega_C} \\
\text{Taking } s = j\omega&, \text{and consider only } H_{high}, \\
\mathcal{L}(y_{in}) &= \frac{1}{H} \cdot \mathcal{L}(y_{out}) \\
\mathcal{L}(y_{in}) &= \frac{1 + s/\omega_C}{s/\omega_C}\mathcal{L}(y_{out}) \\
\mathcal{L}(y_{in}) &= \frac{1}{s/\omega_C}\mathcal{L}(y_{out}) + \mathcal{L}(y_{out}) \\
\therefore y_{in} &= \omega_c \int y_{out} dt + y_{out} \qquad (1)
\end{aligned}$$

where $\mathcal{L}$ is the Laplace Transform of the input or the output. If we perform inverse Laplace Transform by multiplying $1/H$, we can, in principle, recover the input signal, that corresponds to a square pulse.

After optimization, the recovered value corresponds to a a lower cutoff frequency of $f_c = \frac{\omega_c}{2\pi} \approx 2.22$ Hz, which is close to the nominal value given by the company at 3 Hz. An example showing the recovered signal is shown in Fig. 3.

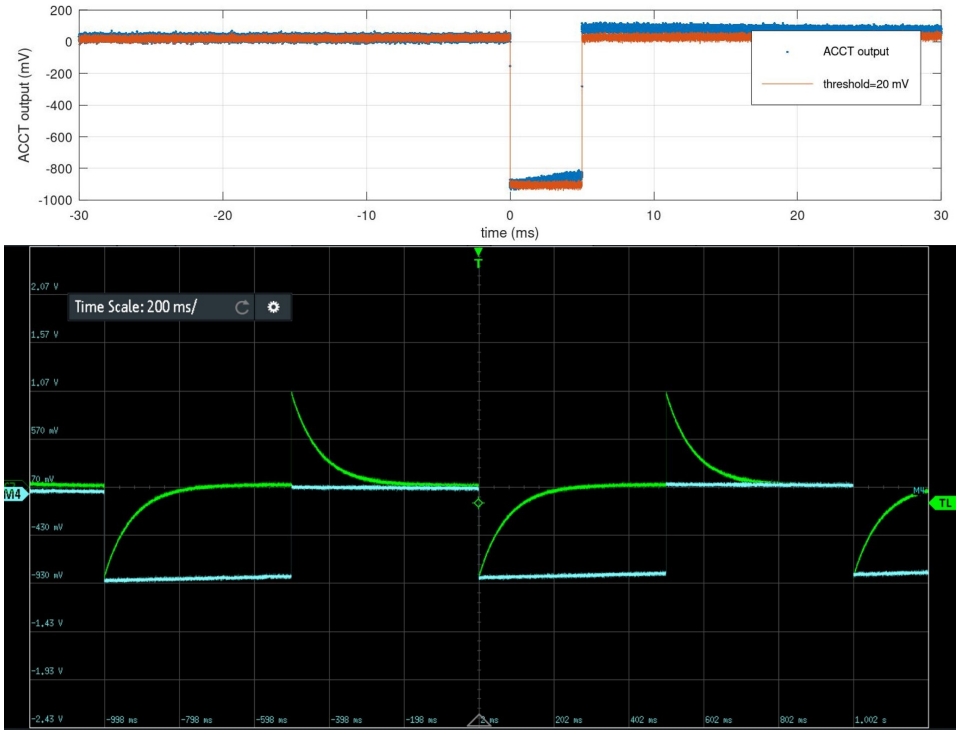

Figure 3: Top figure showing the off-line signal correction with (orange) and without (blue) including the background offset. The bottom figure shows similar correction performed using an oscilloscope on-line.

3.2 Calibration of ACCT

As the peak voltage output from ACCT of different pulse widths (as shown in Fig. 4) are similar, any recovered signal from ACCT should be able to reflect the current flow regardless of the pulse width.

The beam current, I, is calibrated by an external AC source generating a

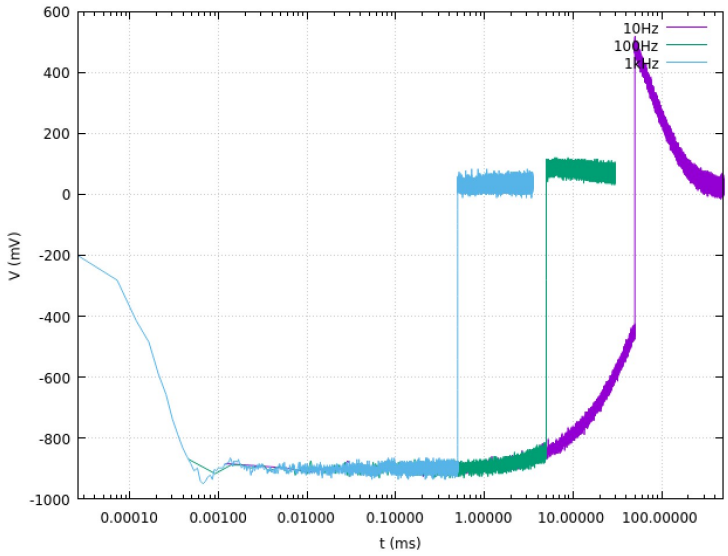

Figure 4: Comparison of ACCT output at the same current but different pulse widths. This shows that the peak V to I relationship is independent of the pulse width, i.e. the calibration should work for any pulse width lying within the band width of the ACCT.

pulse input. The relationship between the output voltage from ACCT, V, and the current flow, I, is shown in Fig. 5. The calibrated function between V and I is given as

$$\mathrm{I\ (mA)} = \mathrm{V\ (mV)} \cdot 0.00106351 - 0.00101202$$

For instance, if the output voltage from ACCT reads 100 mV, the correlated beam current is about 0.1 mA.

3.3 Error estimation

Considering the error of a function f is propagated as

$$\sigma_f^2 = \left(\frac{\partial f}{\partial x_1}\right)^2 \sigma_{x_1}^2 + \left(\frac{\partial f}{\partial x_2}\right)^2 \sigma_{x_2}^2 + \cdots + \left(\frac{\partial f}{\partial x_n}\right)^2 \sigma_{x_n}^2 \tag{2}$$

where x_n represents the n variables involved in f. Since ω_c is the only variable, applying this to equation 1, the standard error, σ of beam current at time t is

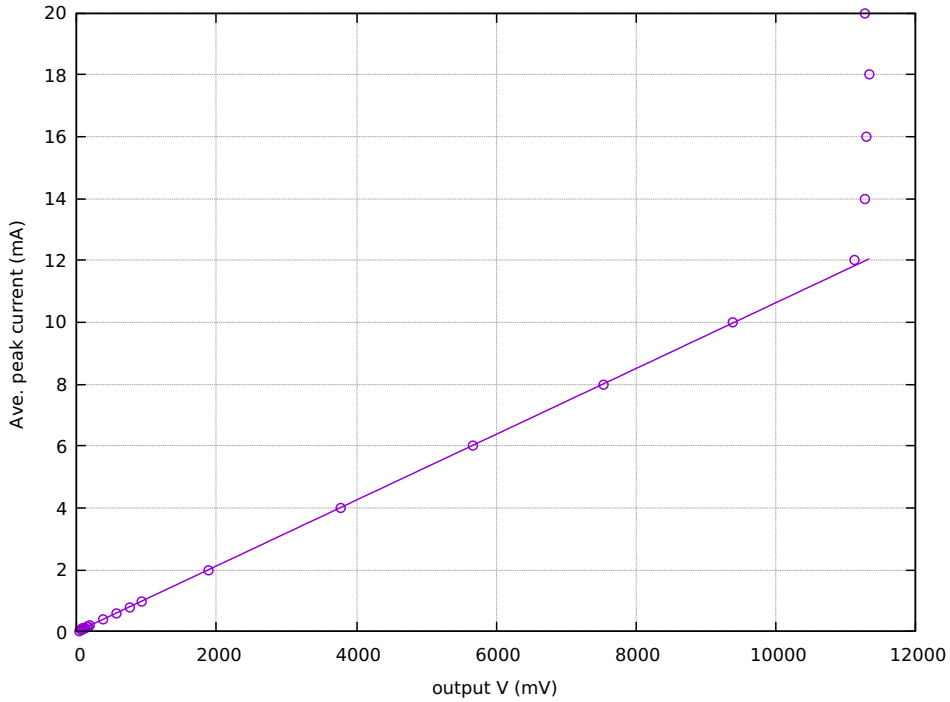

Figure 5: Relationship between the ACCT output voltage and the current running through the calibration winding.

given by

$$
\begin{aligned}
I &= \omega_c \int_{t_o}^{t} y \; dt + y \\
\sigma_I &= \left(\frac{\partial I}{\partial y}\right) \sigma_y \\
\frac{\partial I}{\partial y} &= \omega_c \frac{\partial}{\partial y} \int_{t_o}^{t} y \; dt + \frac{\partial}{\partial y} y \\
&= \omega_c \int_{t_o}^{t} dt + 1 \\
\text{Taking } t_o = 0, \frac{\partial I}{\partial y} &= \omega_c t + 1 \\
\therefore \sigma_I &= (\omega_c t + 1)\sigma_y
\end{aligned} \tag{3}
$$

The standard error will be discussed in the following subsections by taking $\text{Err}_1 = \omega_c t \sigma_y$ and $\text{Err}_2 = \sigma_y$.

3.3.1 Systematic offset correction

Fig. 6 shows an example when the signal transformation was performed without considering any offset correction. The drift is mainly coming from the integral term when performing the transformation to recover the input signal. Such offset usually results in a larger standard deviation and further reducing the accuracy and reliability of the output current.

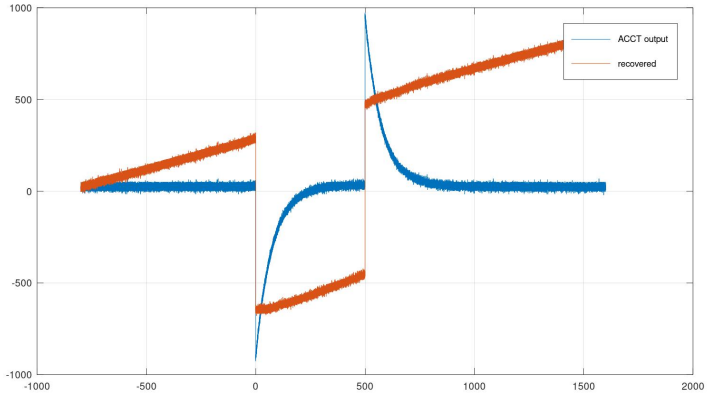

Figure 6: Recovered output without performing any offset correction results in a drift due to the effect of integration during the signal transformation.

Therefore, in order to suppress the error, the offset Δy_{offset} was found by taking the average of the first 10k data from background, then subtracts it from equation 1.

3.3.2 Pulse width dependence

The percentage error at different pulse widths (frequencies) are shown in Fig. 7. From Fig. 7, Err_2 improves when rise time is included in the time interval. This is to reduce the non-linearity at the edge of the pulse, and therefore reduces the standard deviation. Err_2 is significantly high when the pulse width is less than 1 ms. Err_2 constitutes the main error when pulse width is shorter than 100 ms. However, when the pulse width is longer than 100 ms, Err_1 becomes the major contribution of error.

Afterall, a minimal is achieved by including the rise time and having a moderate pulse width T=[0.1,100] ms. For instance, from Fig. 7b, when

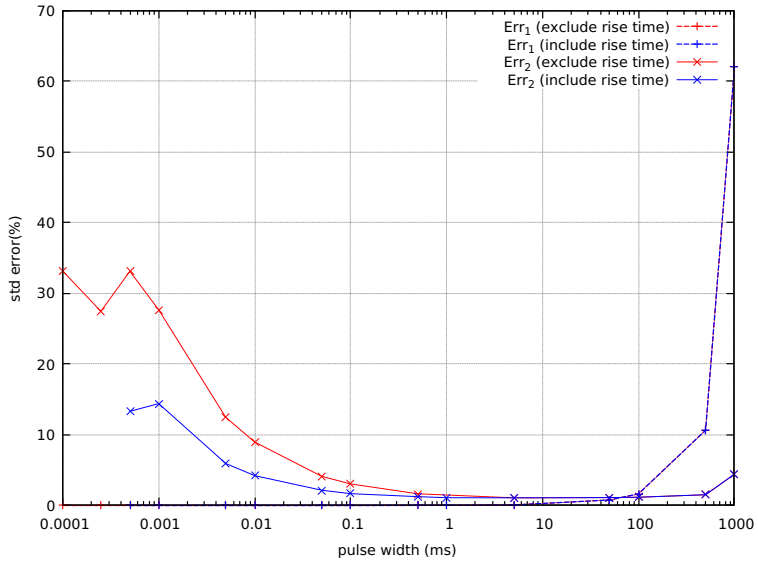

(a) Input peak current = 1 mA

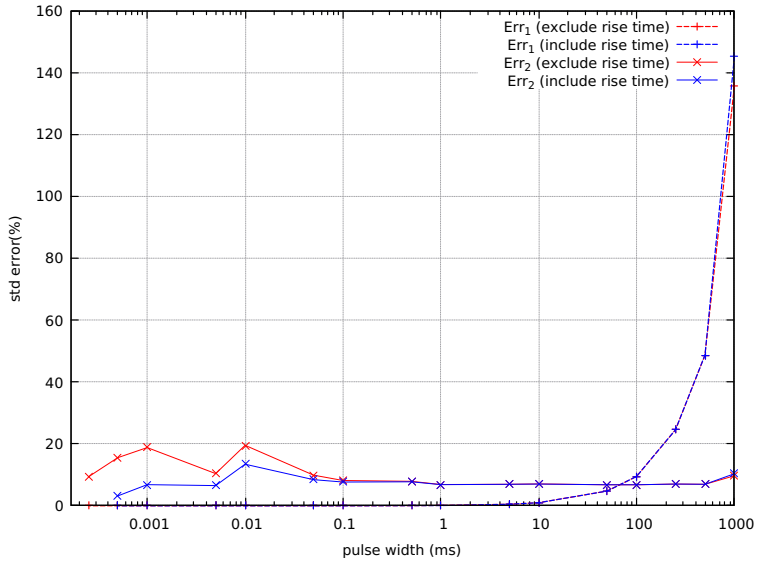

(b) Input peak current = 80 μA

Figure 7: The percentage of error calculated from equation 3 at different pulse widths for an input peak current of 1 mA and 80 μA. The solid lines show the standard deviation from Err_2 on RHS of eqn. 3, while the dashed lines shows the percentage error from Err_1. Red lines has a time interval of [a,b]=[0, pulse width], while the blue lines has a time interval of [a,b]=[RT, pulse width-RT], where RT$\sim$ 150ns. This corresponds to about half of the nominal rise time of $\sim$ 350 ns.

T=10 ms and the average peak current is about 80 μA, the accuracy of the reading is about 8 μA ($\pm$10%). Do also note that this reading does not include any systematic error such as the background (BG) offset etc. Considering a possible error of 2% from the BG, the total error is about $\pm$10 μA for a peak current of 80 μA.

3.3.3 Input current dependence

On top of this, Fig. 8 shows the dependence of standard deviation on the input currents. The standard deviation is large when the current is $<$ 1 mA and the percentage of error remains less than 2% at I$>$ 1 mA. This is due to the background noise that has comparable amplitude with the input signal when the beam current is low.

On the other hand, the ACCT output saturates when the input peak current, I$>$ 12 mA. Therefore, this sets the upper limit of the maximum measurable beam current of this ACCT.

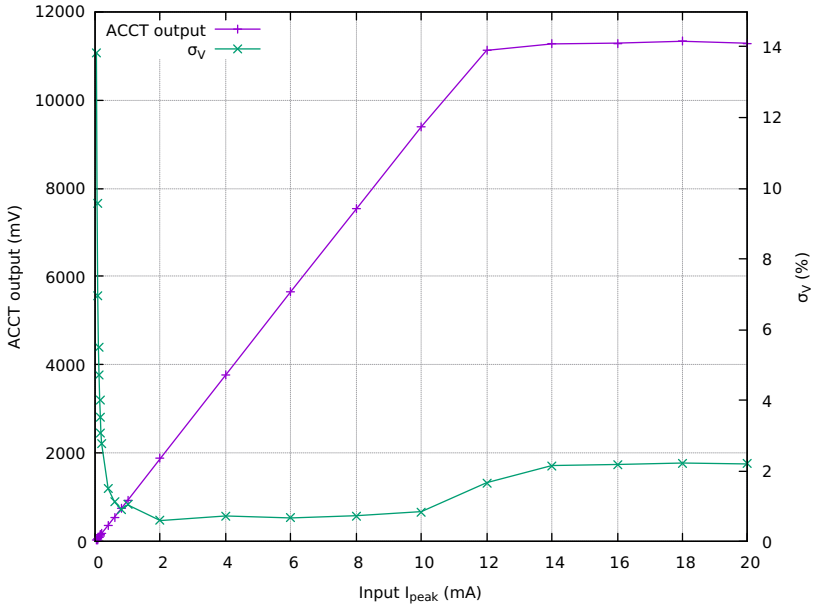

Figure 8: ACCT output including the errorbars at different input peak currents for 5 ms pulse width.

3.3.4 Sampling rate dependence

Furthermore, the sampling rate from ACCT is also investigated. Fig. 9 shows the percentage of error at different sampling rates for 500 ms, 50 ms and 5 ms pulses.

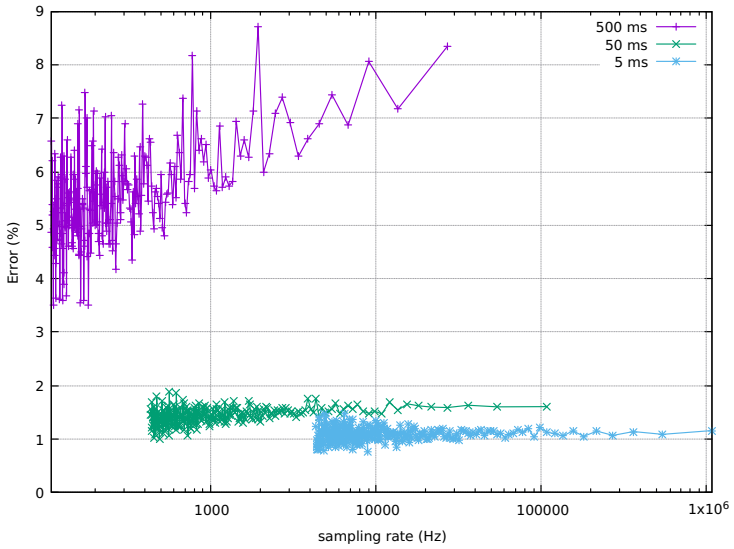

Figure 9: The percentage of error (Err_1+Err_2) at different sampling rate for 500 ms (purple), 50 ms (green) and 5 ms (blue) at 1 mApp.

Generally, the error increases with an increasing sampling rate. This contradicts to the belief that a larger sampling size, N, actually reduces the error. This effect is more prominent for a large pulse with a long pulse width. For instance, the percentage error reduces from about 8% to 4% when the sampling rate is reduced from about 500 kHz to about 100 Hz. Although it is less significant, this is also seen for short pulses such as the 50 ms and 5 ms pulses. Therefore, it is advisable to have the sampling rate kept at around 100 times the beam frequency.

3.3.5 Noise filter dependence

In order to reduce the huge error attributed from the unwanted noise, we investigated the output and its error after applying a noise filter. As shown in Fig. 10, the frequency of background signal is randomly distributed from 0 up to about 55 kHz ($\sim$ sampling frequency). Similarly, this kind of randomized

signals were seen on the pulsed output. The only difference is the peaks at low frequency (< 10 Hz). This aligns with the beam frequency of several Hz. Hence, we can deduce that the random signals at higher frequency are not real, and they are mostly the background or the electronic noise.

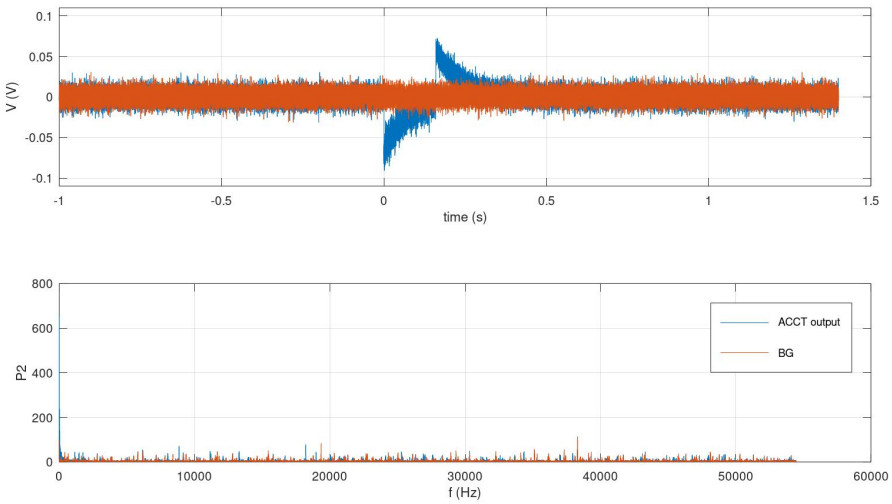

Figure 10: The comparison of the background output (orange) and the output from a 160 ms pulse (blue). The top figure shows the output in time domain, while the bottom figure shows the single sided FFT, P2=magnitude(FFT(V)), in frequency domain.

The effect of applying a finite impulse filter (FIR) to remove the unwanted high-frequency term is shown in Fig. 11. As shown, the filtered output appears to be 'cleaner' with a significant reduction of the background noise.

Fig. 12 shows the dependence of the total error (Err_1+Err_2) upon the cutoff frequency and the order of FIR filter. Generally, σ_I reduces significantly as the cutoff frequency increases, whereas the average peak current remains unchanged. This shows that the filter is effective in cutting off the 'fake' signal but retaining the 'real' output from ACCT. The error converges at about 5 kHz. Therefore, this shall be an optimum cutoff frequency to be applied in future to improve the reliability of this ACCT.On top of this, σ_I is minimum when the order of FIR is about 14. This should be an optimum FIR order to avoid over-filtering.

On the other hand, the results in Fig.12 show that the noise from an e-beam

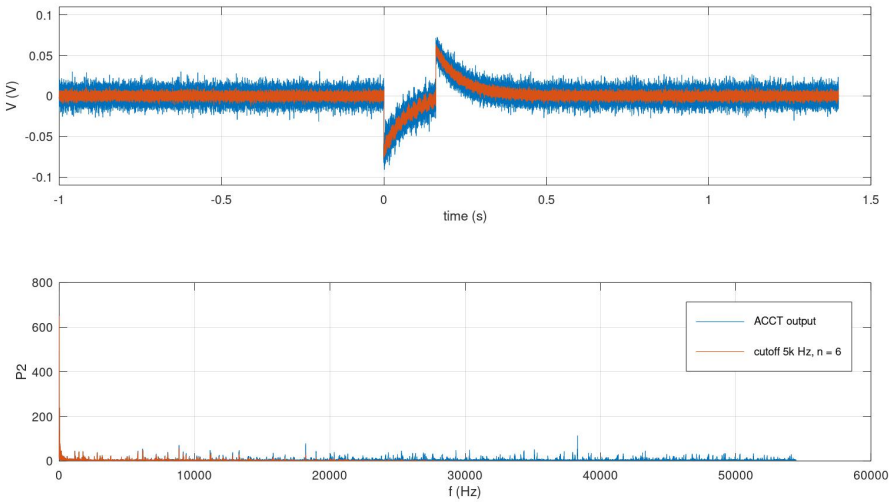

Figure 11: Output signal with (orange) and without (blue) applying FIR filter (up to the 6th order) to cut off components with f $>$ 5 kHz.

is higher than the one from AC source. After applying filter and performing all the correction as mentioned previously, the minimum σ_I for a 100 ms pulse from an AC source is about 6 μA, while the minimum σ_I for a 160 ms pulse for FLASH is about 12 μA.

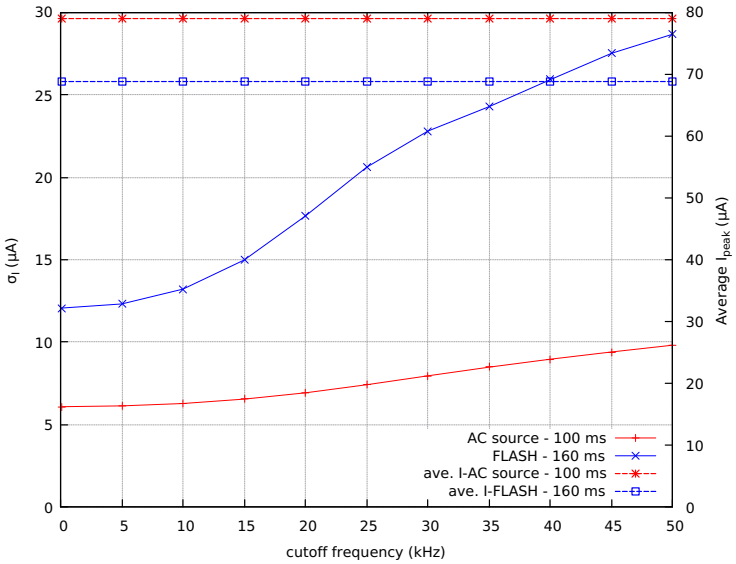

(a) Varying cutfoff frequency

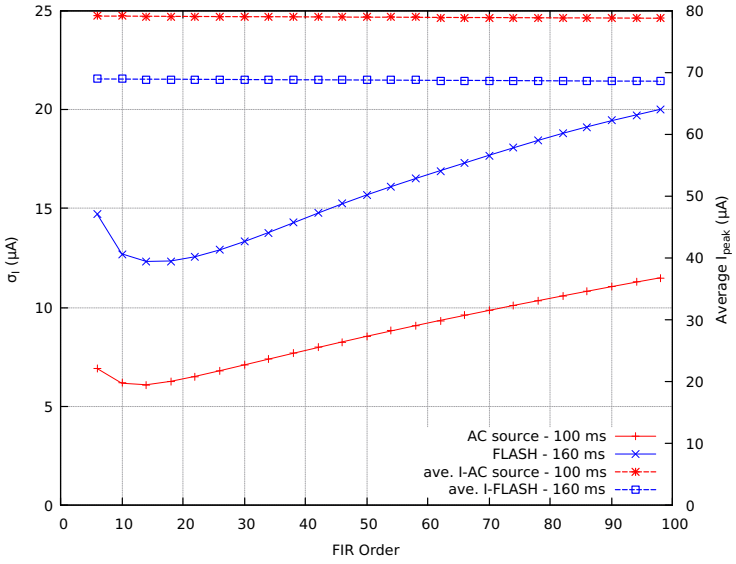

(b) Varying FIR order

Figure 12: The dependence of the total error, (σ_I=Err$_1$+Err$_2$) and average peak current (dashed) on the cutoff frequency and FIR order to suppress the background noise. Blue curve shows the resutls from a real e-beam of 160 ms used for FLASH, while red curve shows the results for a 100 ms pulse from an AC source.

3.4 Examples on Real Applications

Using the above methods and analysis, we tried to recover some data taken for FLASH using a 300 keV electron beam at the ELBT beamline. The e-linac was operating in single pulse mode and the data was collected using the same oscilloscope.

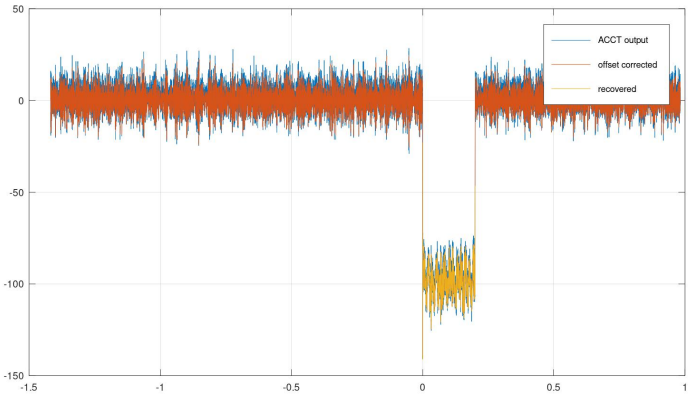

1.

- Date = 2022/03/01
- Frequency = 100 Hz
- Duty Factor = 2%
- Average I = 103.9 ± 8.5 μA

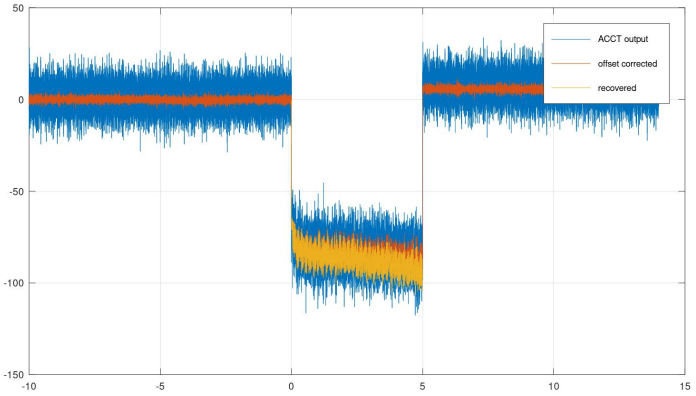

2.

- Date = 2022/03/02
- Frequency = 10 Hz

- Duty Factor = 5%
- Average I = 91.8 ± 7.2 μA

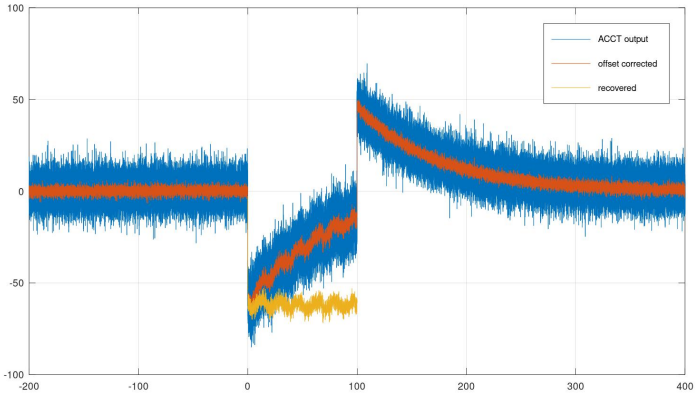

3.

- Date = 2022/03/04
- Frequency = 1 Hz
- Duty Factor : 10%
- Average I : 64.8 ± 7.5 μA

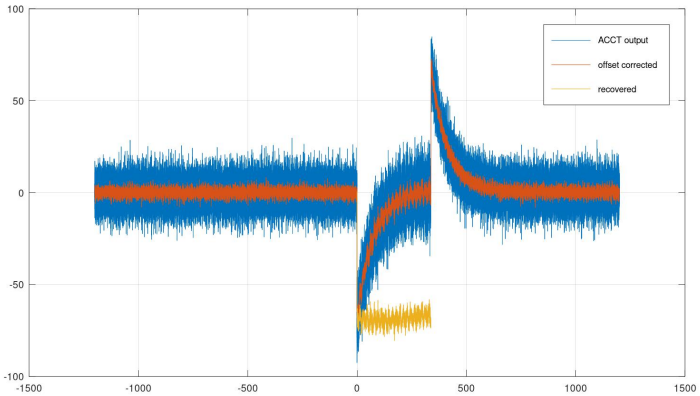

4.

- Date = 2022/03/22
- Frequency = 1 Hz
- Duty Factor = 33.8%

- Average I = $71.8 \pm 20.2\mu$A

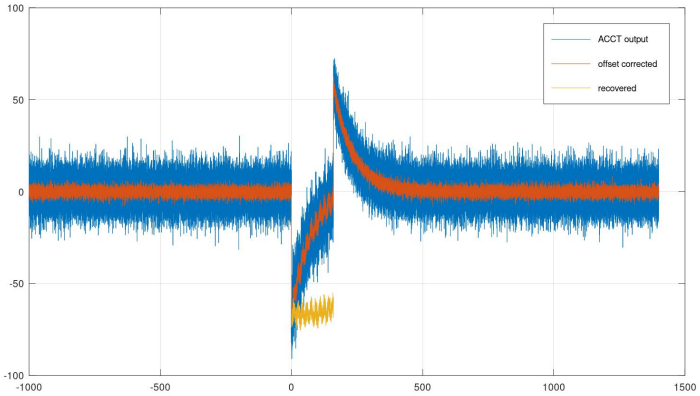

5.

- Date = 2022/03/24
- Frequency = 1 Hz
- Duty Factor = 16.0%
- Average I = 68.9 ± 12.3 μA

4 Summary

To conclude, the ACCT shall perform well with the following conditions:

1. The cutoff frequency for signal recovery, $f_c \approx 2.22$ Hz, which is close to the nominal value given by the company at 3 Hz.
2. Background (BG) offset correction is required when performing signal recovery.
3. The calibrated beam current is about $\frac{1}{1000}$ of the output voltage from ACCT, i.e., 100 mV from ACCT corresponds to a beam current of about 0.1 mA.
4. The optimum operation pulse width should lie within T=[0.1,100] ms, in order to have the maximum accuracy (< 2 % for 1 mA; < 10% for 80 μA).

5. The maximum measurable beam current of this ACCT is 12 mA.

6. A sampling rate of around 100 times the beam frequency is sufficient for this ACCT.

7. Background noise is very effectively suppressed by adding a low-pass filter. For instance, after applying filter at cutoff frequency f=5 kHz for a 160 ms beam used for FLASH, the total error is reduced more than 50%.

5 Appendix

5.1 Specifications of ACCT

- Model name: Bergoz in-air ACCT sensor #ACCT-S-122-CAW1 (1 Turn Calibration Winding, 122 mm ID)
- Full scale range: from 10mA to 2A (factory preset range)
- Ratio accuracy error: <0.1% FS
- Frequency range (-3 dB) : [<3 Hz : 1 MHz]
- Droop: < 2% ms
- Risetime: 350ns (10% - 90%)
- Noise at 10mA F.S.: $\approx .5$ μArms
- Noise at 100mA F.S.: $< 5\mu$Arms
- Bipolar signals. (Positive charges e.g., protons crossing the aperture in the direction of the arrow give a positive output, while negative charges e.g., electrons crossing in the direction of the arrow give a negative output.)
- The cutoff frequency of an ACCT is given by

In order to achieve a low cutoff frequency, the improved Hereward principle is implemented in this ACCT (as shown in Fig. 14).

The lower frequency cutoff (-3 dB) of a transformer is given by:

$$f_L = \frac{R}{2\pi \cdot L}$$

Where:

- L is the core winding inductance
- R is the winding load

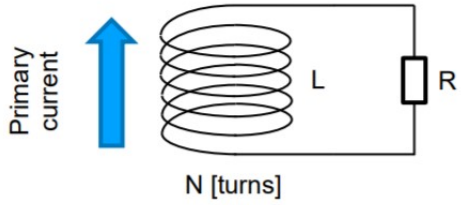

Figure 13: Measurement of curoff frequency in ACCT. -3 dB corresponds to a cutoff when the voltage drops more than 70.71% of the input voltage.

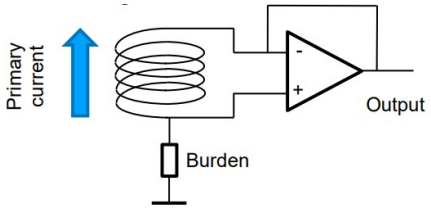

Figure 14: A simplified circuit diagram showing an improvement made by K. Unser in 1963 from the Hereward transformer principle. The ACCT in this work implements this working principle to suppress the ACCT offset voltage to very close to zero when no primary current flows thru the sensor.

The frequency response of the ACCT in detecting a 1 mA peak current flowing into the CAL winding is shown in Fig. 15.

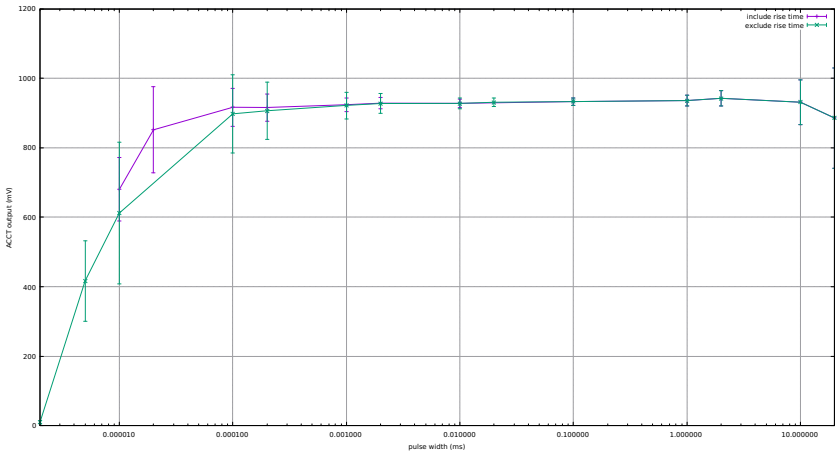

Figure 15: The frequency response of ACCT output (with errorbars) at different pulse widths using a pulse of 1 mA peak current.

5.2 Comparison of Simpson's and Trapezoid Integral

Two different numerical integral were compared during the signal recovery. They are the composite Simpson's method and the trapezoid method. A comparison of the output from both methods are shown in Fig. 16. As shown, the percentage difference between these two methods is small ($< 1.5\%$). Therefore, in order to reduce the computational time, the trapezoid integral was used.

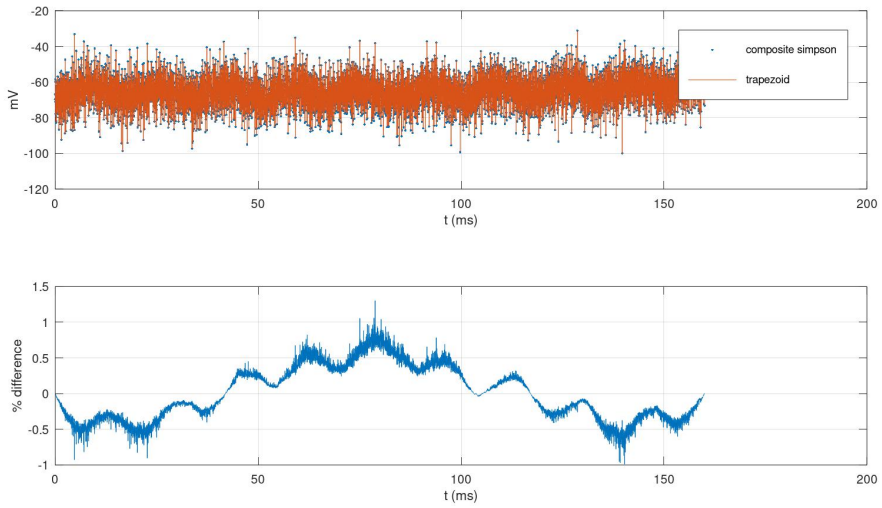

Figure 16: Comparison of recovered signals using two difference integrals. The top figure shows the recovered output from Simpson's rule (blue) and trapezoid integration (orange). The lower figure shows the percentage difference between these two method.